Japan Journal of Research

Original Article

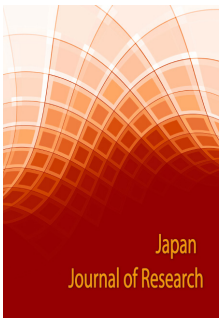

Electrical and Thermal Simulations of a Lithium-Ion Battery Cell: A Comparative Study of Commercial Software Platforms

Yiqun Liu

College of Engineering Technology, Ferris State University, Big Rapids, Michigan, USA

Correspondence

Prof. Dr. Yiqun Liu

College of Engineering Technology, Ferris State University, Big Rapids, Michigan, USA

- Received Date: 02 Jan 2025
- Accepted Date: 15 Jan 2025
- Publication Date: 18 Jan 2025

Keywords

Lithium-ion battery modeling; Battery simulation software; MATLAB/Simulink; COMSOL Multiphysics; ANSYS Fluent.

Abstract

Commercial software tools have become essential for modeling and simulating lithium-ion batteries, offering researchers and engineers powerful platforms to analyze battery behavior under various operating conditions. Among the most widely used tools are MATLAB/Simulink, COMSOL Multiphysics, and ANSYS Fluent, each offering unique capabilities for electrical and thermal simulations. MATLAB/Simulink is popular for its user-friendly environment and fast execution of simplified lumped-parameter models, while COMSOL Multiphysics and ANSYS Fluent enable detailed, physics-based simulations with higher spatial resolution. In this paper, the performance of MATLAB/Simulink, COMSOL Multiphysics, and ANSYS Fluent is compared by modeling and simulating a lithium-ion polymer battery cell designed for electric vehicle applications. All the parameters required for model development are obtained from experimental data. MATLAB/Simulink is used to simulate the effects of terminal current and ambient temperature on the battery's discharge voltage and usable capacity. COMSOL Multiphysics and ANSYS Fluent are employed to simulate cell terminal voltage and temperature distribution profiles over the battery cell surface under various continuous charge and discharge conditions. Additionally, ANSYS Fluent is used to model the surface temperature distribution caused by an internal short-circuit resulting from foreign object penetration. The simulation results are validated using experimental data, showing good agreement for both electrical and thermal behavior under different loading and ambient conditions. The comparison highlights that MATLAB/Simulink is particularly well-suited for quick, zero-dimensional lumped simulations of battery electrical and thermal responses due to its simplicity and computational efficiency. In contrast, COMSOL Multiphysics and ANSYS Fluent involve more complex model setups but offer significant advantages for performing detailed three-dimensional simulations, capturing spatial distributions of current and temperature across the battery cell. These insights are valuable for selecting the appropriate simulation tool based on the complexity and goals of battery modeling applications.

Introduction

The rapid expansion of the electric vehicle sector in the past 15 years has significantly accelerated advancements in battery modeling and simulation software. This surge is a response to increasing demands for powerful tools capable of solving challenges related to battery system design, battery management systems, and thermal management systems. Prominent software solutions, including MATLAB/Simulink [1-4], COMSOL Multiphysics [5-8], and ANSYS [9-12], have emerged as essential platforms for engineers and researchers, enabling design optimization for lithium-ion batteries, modules, and packs, as well as simulations for energy grids, aging effects, and abuse conditions.

Commercial simulation tools play a key role in the design and development of batteries for electric vehicles, hybrids, and industrial applications. These platforms allow engineers to analyze physical, chemical, and thermal battery behaviors to enhance performance, safety, and efficiency. As battery systems have become increasingly complex, the need for advanced simulation technologies has grown exponentially.

A core aspect of battery system design involves understanding the interactions between the battery and other vehicle components such as electric motors, power electronics, braking, and cooling systems. MATLAB/Simulink has emerged as a leading solution in this domain, enabling dynamic system modeling through modular subsystems like battery modules, thermal management systems, and electric drivetrains. Tools like ADVISOR enhance Simulink's capabilities, while platforms such as GT-Suite offer specialized features for thermal and co-simulation tasks. MATLAB/Simulink has become a preferred platform for developing and testing battery management systems (BMS). A BMS is critical for ensuring safe and efficient battery operation by monitoring parameters like voltage, current, temperature, and state-of-charge (SOC). Simulink's support for real-time simulation and model-based design allows engineers to create,

Citation: Liu Y. Electrical and Thermal Simulations of a Lithium-Ion Battery Cell: A Comparative Study of Commercial Software Platforms. Japan J Res. 2025;6(4):108.

test, and validate BMS algorithms effectively. Simulink enables engineers to integrate battery pack models with thermal and electrical subsystems, facilitating performance analysis under different operating scenarios. The software's extensive library of prebuilt modules accelerates the design process, minimizes development costs, and supports robust system validation. Widely adopted in both academia and industry, MATLAB/Simulink remains an essential tool for system-level battery simulations.

In contrast to MATLAB/Simulink's system-level focus, COMSOL Multiphysics specializes in detailed physics-based simulations of battery behavior. With its battery module, COMSOL allows for accurate modeling of lithium-ion batteries by incorporating complex electrochemical, thermal, and mechanical processes. Engineers can analyze phenomena such as ion transport, heat generation, and thermal runaway, providing critical insights for battery performance under varying conditions, including rapid charging and extreme temperatures. COMSOL's unique ability to define custom model equations has made it particularly popular among researchers who require flexibility in exploring advanced battery behaviors. This includes simulations of battery degradation, capacity loss, and internal faults like short-circuits. Additionally, its multi-scale modeling capabilities bridge the gap between material-level properties and large-scale battery performance, enabling more precise optimization of cell design and safety. The software also supports coupled simulations that combine thermal, electrochemical, and mechanical analyses, allowing engineers to predict battery behavior under abuse conditions such as mechanical stress, overcharging, and thermal expansion. These capabilities are crucial for improving battery durability and safety.

ANSYS provides a comprehensive toolkit for modeling and analyzing batteries, particularly focusing on electrothermal performance and mechanical behavior. ANSYS Fluent, a leading computational fluid dynamics (CFD) tool, is widely used to design and optimize battery thermal management systems. ANSYS Fluent's capabilities include detailed simulations of heat generation, dissipation, and fluid dynamics, ensuring optimal thermal regulation in battery packs. A standout feature of ANSYS is its implementation of the Multi-Scale Multi-Domain (MSMD) framework, developed by the National Renewable Energy Laboratory (NREL). This framework enables accurate simulations of heat generation, ion transport, and charge-transfer processes within lithium-ion cells, making it invaluable for optimizing energy density, thermal stability, and overall lifespan. ANSYS further offers LS-DYNA, a powerful tool for mechanical simulations, such as predicting battery behavior during crash tests, impacts, and abuse scenarios. LS-DYNA's ability to model mechanical deformation and failure under extreme conditions is critical for ensuring the safety and reliability of automotive battery systems.

The ongoing growth of the electric vehicle market has created a strong synergy between software innovation and the battery industry. Advancements in simulation tools allow for increasingly efficient and safer battery designs, while industry demand continues to push for new capabilities. Looking ahead, battery simulation tools are expected to evolve even further. Innovations such as real-time monitoring, enhanced microstructural modeling, and integrated mechanical-thermal simulations will become standard practices. These tools will continue to support the industry's drive for batteries with improved energy density, longer life cycles, and enhanced safety.

Overall, commercial software solutions have become indispensable for battery design, modeling, and simulation. MATLAB/Simulink dominates in system-level modeling, COMSOL excels at detailed physics-based simulations, and ANSYS provides integrated tools for electrothermal and mechanical analysis. Together, these platforms empower engineers to overcome the challenges of modern battery systems, facilitating advancements in energy storage technology and supporting the future of electric vehicles.

In this paper, three commercial software tools—MATLAB/Simulink, COMSOL Multiphysics, and ANSYS Fluent—are utilized to model and simulate a lithium-ion polymer battery cell for electric vehicle applications. All parameters required for the model setup are derived from experimental data obtained from the battery cell.

MATLAB/Simulink is employed to analyze the effects of terminal current and ambient temperature on the battery cell's discharge voltage and usable capacity. COMSOL Multiphysics and ANSYS Fluent are used to simulate the cell voltage and temperature distribution across the cell surface under various continuous charge and discharge conditions. Additionally, ANSYS Fluent is specifically applied to model the cell surface temperature distribution following an internal short-circuit caused by foreign object penetration.

The simulated results from all three tools are validated against experimental data. The similarities, differences, and strengths of each modeling approach are discussed comprehensively at the end of the paper.

The rest of this paper is organized as follows:

1. Section 2 describes the battery testing equipment, the parameters and specifications of the battery cell, and the experimental procedures.
2. Sections 3, 4, and 5 present the development, simulation results, and validation of the battery cell models in MATLAB/Simulink, COMSOL Multiphysics, and ANSYS Fluent, respectively.
3. Section 6 provides a comparative discussion of the modeling approaches, highlighting their similarities, differences, and strengths, and conclude the paper with a summary of findings.

Experiments of the Lithium-ion Battery Cell

The experimental setup contains a Digatron charge/discharge unit (cycler) and an Envirotronics temperature chamber. The charge/discharge unit is operated through Battery Manager software, which enables the creation and execution of various testing protocols, including continuous, pulse, and dynamic charging/discharging profiles based on driving cycle data. The software efficiently monitors and records critical parameters such as current, voltage, and energy (in ampere-hours) charged or discharged, with a high temporal resolution of up to 0.1 seconds.

The Envirotronics temperature chamber ensures a stable and controlled ambient environment for battery testing, offering an internal temperature range from -70°C to 180°C. Its interior is constructed with steel plates, and the observation window consists of five-layer high-strength glass, ensuring a secure environment even in cases of thermal runaway or explosion.

For monitoring the surface temperature of the battery cells, OMEGA SA1-K-SRTC surface thermocouples with self-

adhesive backing are utilized. These thermocouples provide precise temperature measurements with a maximum limit of 175°C and a fast response time of 0.3 seconds. They are connected to TEKCOPLUS 4-channel K-type thermocouple meters (model THTK-6), which display real-time data and record temperature readings at 1-second intervals.

The battery cells tested in this study are EiG ePLB-C020 pouch-type lithium-ion polymer cells. These cells feature a nominal capacity of 20 Ah and a nominal voltage of 3.6 V. They utilize a Lithium-Nickel-Manganese-Cobalt-Oxide (LiNiMnCoO2) cathode and a graphite-based anode, making them well-suited for applications in plug-in hybrid electric vehicles (PHEVs) and electric vehicles (EVs).

Figure 1 provides an overview of the testing equipment and experimental setup, while the specifications of the battery cells and their components are detailed in Tables 1 and 2.

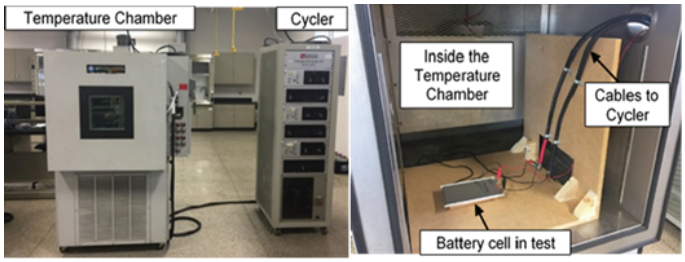

Figure 1. *Experimental setup of the battery testing: Cycler and temperature chamber (left); Battery cell testing inside the temperature chamber (right).*

Table 1. *Specifications of EiG ePLB-C020 battery cell.*

Length	196 mm
Width	127 mm
Thickness	7 mm
Weight	428 g
Nominal voltage	3.6 V
Nominal capacity	20 Ah
AC impedance (1 kHz)	<3 mΩ
Specific energy	174 Wh/kg
Energy density	370 Wh/L
Specific power (50% DOD, 10 seconds)	2300 W/kg
Power density (50% DOD, 10 seconds)	4600 W/L
Maximum charging voltage	4.15 V
Lower voltage limit for discharge	2.5 V

Table 2. *Specifications of EiG ePLB-C020 battery cell components.*

Material/Layer	Thickness (μm)	No. of Layers	Density (kg/m^3)
Aluminum foil	21	17	2702
Copper foil	12	18	8933
Separator sheet	25	36	1017 (wet)
Positive electrode	70	34	2895 (wet)
Negative electrode	79	36	1555 (wet)

The surface temperature distributions of the battery cell are measured under continuous charging (20A and 40A) and discharging (20A, 40A, 60A, and 80A) conditions. Eight OMEGA thermocouples are attached to specific surface locations and connected to TEKCOPLUS meters, as shown in Figure 2. Inside the temperature chamber set to 25°C, the cell is fully charged to 4.2V using 20A, followed by a constant voltage charging method. After stabilizing around 27°C, discharging begin, and temperature data are recorded every 30 seconds. This process is repeated for different discharging and charging currents, with voltage-controlled steps at 2.5V for discharging and 4.2V for charging.

Experiments on internal short-circuit caused by object penetration in battery cells are also performed, as shown in Figure 3. The effects of initial SOC levels (10%, 50%, and 90%) and penetration locations on cell temperature and terminal voltage variations are examined using nine cells. Before testing, each cell is fully discharged to 2.5V at a 1C-rate and then charged to the desired SOC levels. A Mark-10 ESM 301 motorized stand with a 12 mm diameter, 60° cone is used to penetrate the cells at 28 mm/min, completing penetration in 15 seconds. Surface temperatures and terminal voltages are measured during tests, with data recorded every 30 seconds.

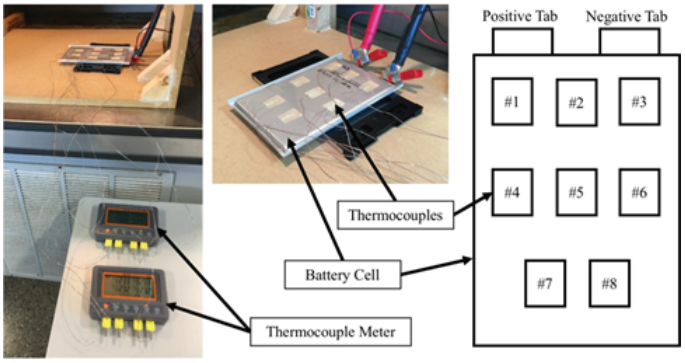

Figure 2. *Experimental setup for the battery surface temperature measurement and the locations of the thermocouples on the battery cell surface.*

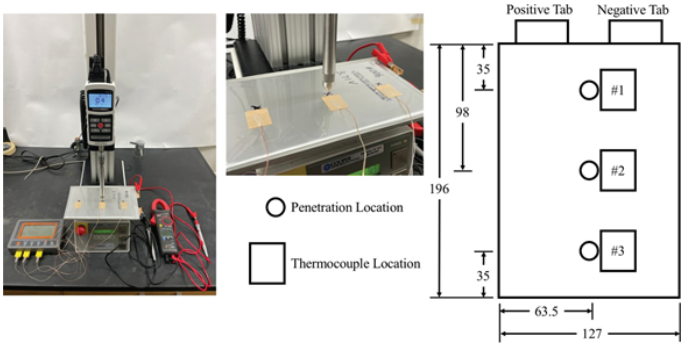

Figure 3. *Penetration test setup (left), closer look of penetrating cone (middle), and penetration locations and thermocouple locations with unit in mm (right).*

Zero-dimensional (0-D) Battery Model Developed in MATLAB/Simulink

The 0-D electro-thermal model of the battery cell utilized in this section is built using the "battery" block from the Simulink library, which offers a detailed representation of the battery's electro-thermal behavior. Although the model can accurately simulate factors like ambient temperature effects and battery

aging, it relies on experimental data for calibration to match a specific battery type. This section primarily focuses on analyzing how ambient temperature influences the battery's performance.

Equations (1) to (6) [13] are incorporated into the "battery" block to model the influence of temperature on the battery parameters during the discharge process (i*> 0).

$$f_1(it,i^*,i,T,T_a) = E_0(T) - K(T)\cdot\frac{Q(T_a)}{Q(T_a)-it}\cdot(i^*+it) + A\cdot\exp(-B\cdot it) - C\cdot it \quad (1)$$

$$V_{batt}(T) = f_1(it,i^*,i,T,T_a) - R(T)\cdot i \quad (2)$$

with

$$E_0(T) = E_0|_{T_{ref}} + \frac{\partial E}{\partial T}(T - T_{ref}) \quad (3)$$

$$K(T) = K|_{T_{ref}}\cdot\exp\left[\alpha\left(\frac{1}{T}-\frac{1}{T_{ref}}\right)\right] \quad (4)$$

$$Q(T_a) = Q|_{T_a} + \frac{\Delta Q}{\Delta T}\cdot(T_a - T_{ref}) \quad (5)$$

$$R(T) = R|_{T_{ref}}\cdot\exp\left[\beta\left(\frac{1}{T}-\frac{1}{T_{ref}}\right)\right] \quad (6)$$

Where

it is extracted capacity, in Ah;

i^* is low frequency current dynamics, in A;

i is battery current, in A

T is cell or internal temperature, in K;

T_a is ambient temperature, in K;

E_0 is constant voltage, in V;

K is polarization constant, in V/Ah, or polarization resistance, in Ohms;

Q is maximum battery capacity, in Ah;

A is exponential voltage, in V;

B is exponential capacity, in Ah^{-1};

C is nominal discharge curve slope, in V/Ah;

V_{batt} is battery voltage, in V;

R is battery internal resistance, in Ohms;

T_{ref} is nominal ambient temperature, in K;

E/T is reversible voltage temperature coefficient, in V/K;

α is Arrhenius rate constant for the polarization resistance;

β is Arrhenius rate constant for the internal resistance;

$\Delta Q/\Delta T$ is maximum capacity temperature coefficient, in Ah/K.

The equations above illustrate that the battery's charging and discharging voltage is affected by multiple factors, such as the constant voltage, polarization constant, maximum battery capacity, and internal resistance—all of which depend on temperature, either the cell temperature or the ambient temperature. Furthermore, the exponential voltage, exponential capacity, and the slope of the nominal discharge curve also play a role in determining the battery voltage.

The procedure for creating the model in the Simulink platform [13] is summarized as follows. First, the "simulate temperature effect" option is selected in the battery setup dialog, which opens the temperature tab. This tab requires parameters determined from a discharging test conducted at ambient temperatures below 20°C. In this case, data from a 20A discharge test at 0°C is used. The "initial cell temperature (°C)" is set to the ambient temperature, as the battery has equilibrated to this temperature before testing. The "nominal ambient temperature T1 (°C)" is assumed to be 20°C, representing standard conditions. The "second ambient temperature T2 (°C)" is set to 0°C to simulate a colder operating condition. At T2, the "maximum capacity (Ah)" is 16Ah, and the "initial discharge voltage (V)" is set to 3.75V. The "voltage at 90% maximum capacity (V)" is 3.07V, and the "exponential zone (voltage-V, capacity-Ah)" values are 3.59V and 3.6Ah, respectively. Key model parameters, derived from experimental discharge curves, are presented in Figure 4 and Table 3. The final 0-D model, which accounts for ambient temperature effects, is shown in Figure 5.

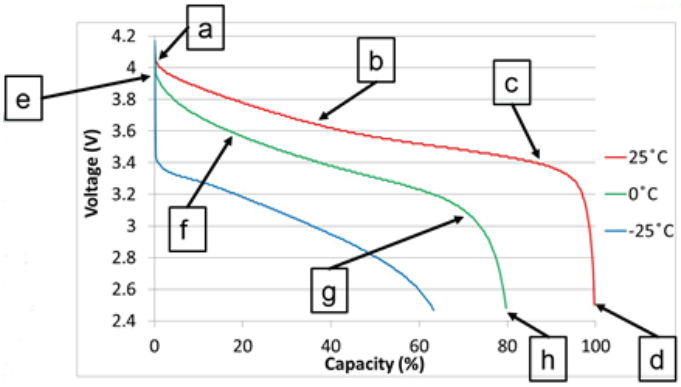

Figure 4. *Kay parameters used for developing the MATLAB/Simulink battery cell model.*

Table 3. *Kay parameters used for developing the MATLAB/Simulink battery cell model.*

a	Fully charged voltage	4.04V
b	Exponential zone	[3.64V; 7.4Ah]
c	Voltage and capacity at end of nominal area	[3.39V; 18Ah]
d	Maximum capacity	20Ah
e	Initial discharge voltage at 0 °C	3.95V
f	Exponential zone at 0 °C	[3.59V; 3.6Ah]
g	Voltage at 90% maximum capacity at 0 °C	3.07V
h	Maximum capacity at 0 °C	16Ah

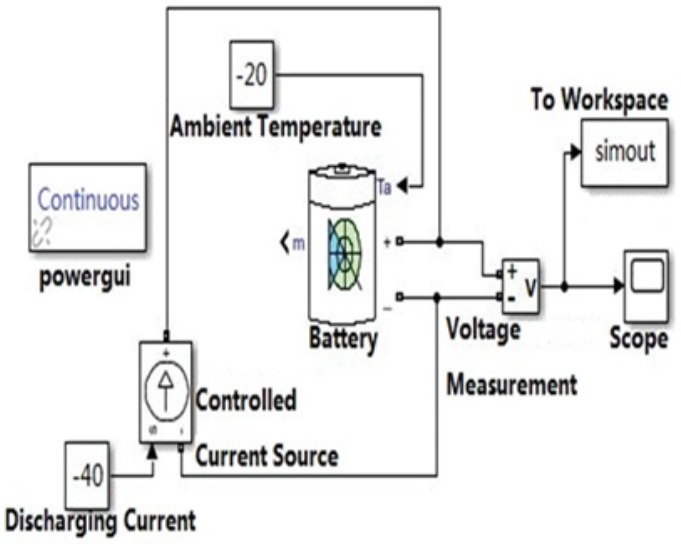

Figure 5. *Battery cell model developed in MATLAB/Simulink.*

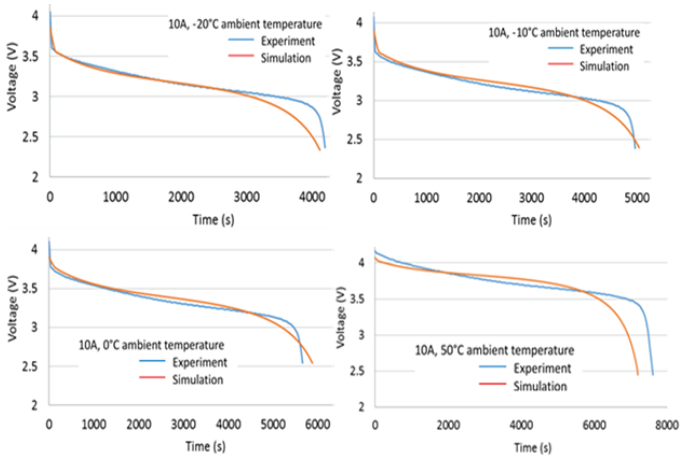

Figure 6. *Discharging voltage comparisons at 10A discharging current between experimental and Simulink simulated data.*

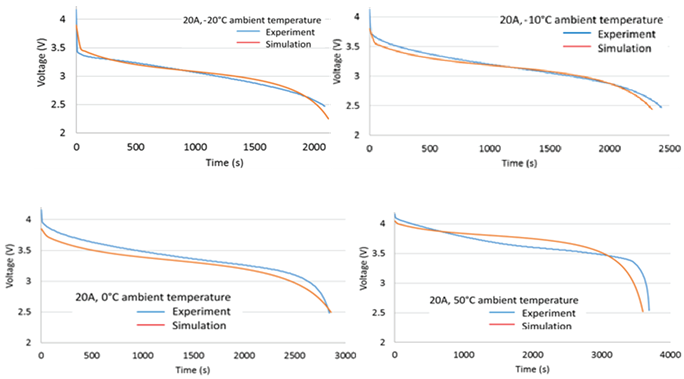

Figure 7. *Discharging voltage comparisons at 20A discharging current between experimental and Simulink simulated data.*

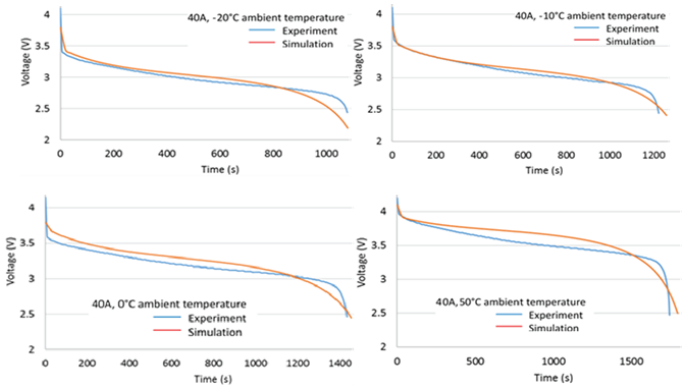

Figure 8. *Discharging voltage comparisons at 40A discharging current between experimental and Simulink simulated data.*

The Simulink model is validated and correlated using the previously described experimental setup, involving 12 discharging tests at constant currents of 10A, 20A, and 40A under four ambient temperatures: -20°C, -10°C, 0°C, and 50°C. The simulated discharge curves are compared to the corresponding experimental curves, as shown in Figures 6, 7, and 8. The results indicate a close alignment between experimental and simulated curves from 0% to 80% depth-of-discharge (DOD), with deviations generally below 7%. However, discrepancies increase beyond 80% DOD, likely due to the model parameters being based on a nominal voltage of 3.6V, which does not fully capture the voltage drop at higher discharge levels. Despite this, the model demonstrates reliable accuracy within the 0%–80% DOD range, which is where batteries are typically operated. The simulated and experimental discharging times to reach the cutoff voltage of 2.5V show good correlation in most cases. At higher ambient temperatures (50°C), the experimental results reveal an increase in usable capacity, leading to extended discharge times—over 2 hours for the 10A test and over 1 hour for the 20A test. However, the Simulink model does not account for this temperature-driven capacity increase, causing the simulations to terminate at 3600 seconds for the 1C discharge and 1800 seconds for the 2C discharge, underestimating the actual discharge duration.

One-dimensional (1-D) and Three-dimensional (3-D) Battery Models Developed in COMSOL Multiphysics

The electrochemical approach to battery modeling focuses on the detailed particle motion and chemical reactions occurring within the battery. This type of model is particularly suited for optimizing battery design, including voltage, current, energy characteristics, and determining design specifications, as it emphasizes the physical properties of the battery's structure and materials. A typical electrochemical model involves a set of coupled partial differential and algebraic equations that describe particle behavior in the electrode regions, linked by boundary conditions. Solving these models requires substantial computational resources, but they can provide highly accurate results if detailed battery specifications are available. This section discusses the modeling and validation of a lithium-ion battery cell using the COMSOL Multiphysics platform.

The governing equations from [14] are applied to each component in the COMSOL lithium-ion battery model. Equation 7 represents the general mass balance for the diluted species in the electrolyte for each species i. The flux of ions in the electrolyte is described by the Nernst-Planck equations, which account for ion transport through diffusion, migration, and convection. These three processes correspond to the first, second, and third terms on the right-hand side of Equation 8, respectively.

$$\frac{\partial c_i}{\partial t} + \nabla \bullet \boldsymbol{N}_i = R_i \qquad (7)$$

$$\boldsymbol{N}_i = -D_i \nabla c_i - z_i u_{m,i} F c_i \nabla \varphi_l + c_i \boldsymbol{u} \qquad (8)$$

where

c_i is the concentration of the ion i (SI unit: mol/m^3),

z_i is the valence,

D_i is the diffusion coefficient (SI unit: m^2/s),

$u_{m,i}$ is its mobility (SI unit: s·mol/kg),

F is the Faraday constant (SI unit: C/mol),

φ_l is the electrolyte potential (SI unit: V), and

$\boldsymbol{u}$ is the velocity vector (SI unit: m/s).

The current density vector $\boldsymbol{i}_l$ in the electrolyte (SI unit: A/m^2) can be described using the sum of all species fluxes:

$$\boldsymbol{i}_l = F \sum z_i \boldsymbol{N}_i \qquad (9)$$

Under the assumptions of electroneutrality, which causes the convection term to vanish, and negligible concentration gradients of the current-carrying ion, which causes the diffusion term to be disregarded, the expression for the current density vector in the electrolyte simplifies to the following:

$$\boldsymbol{i}_l = -F^2 \sum z_i^2 u_{m,i} c_i \nabla \varphi_l \qquad (10)$$

Further, if assuming approximately constant composition of charge carriers, a constant electrolyte conductivity can be defined as:

$$\sigma_l = F^2 \sum z_i^2 u_{m,i} c_i \qquad (11)$$

so the current density in the electrolyte can be written as:

$$\boldsymbol{i}_l = -\sigma_l \nabla \varphi_l \qquad (12)$$

This equation resembles Ohm's law, with charge transport in the electrolyte behaving in an ohmic manner under the given assumptions. Charge conservation leads to the domain equation typically used for the electrolyte in the Primary and Secondary Current Distribution interfaces:

$$\nabla \cdot \boldsymbol{i}_l = 0 \qquad (13)$$

The Primary and Secondary Current Distribution interfaces define two dependent variables: one representing the potential in the electrolyte and the other representing the electric potential in the electrode. In the electrolyte, current conduction is assumed to occur via ion transport, as previously described, while in the electrode, current is conducted by electrons. Since Ohm's law governs current conduction in the solid electrode phase as well, the general equation for the electrodes is given by:

$$\nabla \cdot \boldsymbol{i}_s = Q_s \qquad (14)$$

with

$$\boldsymbol{i}_s = -\sigma_s \nabla \varphi_s \qquad (15)$$

where $\boldsymbol{i}_s$ is the current density vector in the electrodes, and Q_s is a general source term. σ_s denotes the electrode conductivity (SI unit: S/m) and φ_s is the potential of the electrodes (SI unit: V).

The governing equations from [14] are used to model the electrochemical heating:

$$\rho C_p \frac{\partial T}{\partial t} + \rho C_p \boldsymbol{u} \cdot \nabla T = \nabla \cdot (k \nabla T) + Q_h \qquad (16)$$

$$Q_h = Q_{JH} + \sum_m a_{v,m} Q_m \qquad (17)$$

$$Q_{JH} = -(\boldsymbol{i}_s \cdot \nabla \varphi_s + \boldsymbol{i}_l \cdot \nabla \varphi_l) \qquad (18)$$

$$Q_m = (\varphi_s - \varphi_l - E_{eq,m} + T \frac{\partial E_{eq,m}}{\partial T}) i_{loc,m} \qquad (19)$$

where:
ρ is the density;
C_p is the specific heat capacity;
k is the thermal conductivity;
Q_h is the additional heat sources;
Q_{JH} is the joule heating source term;
$a_{v,m}$ is the specific surface area;
Q_m is the local heat source;
E_{eq} is the equilibrium potential;
i_{loc} is the local charge transfer current density.

The additional heat sources, Q_h, in Equation 16 include both the joule heating term and the local heat generation. As shown in Equation 18, the joule heating source arises from charge transport within the solid conductor material and the electrolyte. Equation 19 expresses the total overpotential, $\varphi_s - \varphi_l - E_{eq,m}$ which represents the local heat source resulting from the electrochemical conversion process.

A 1-D electrochemical battery cell model is developed using the COMSOL Multiphysics platform, as shown in Figure 9. This model represents the battery as a linear structure consisting of three distinct sections: the NMC positive electrode, which uses LiNi1/3Mn1/3Co1/3O2 material; the graphite negative electrode, made from LixC6 MCMB material; and the LiPF6 polymer electrolyte. The dimensions of each section, corresponding to the thickness of the battery's components, are based on the specifications of the tested battery cell, ensuring that the model accurately reflects the actual geometry of the cell.

The simulation results of the discharge voltage curves for

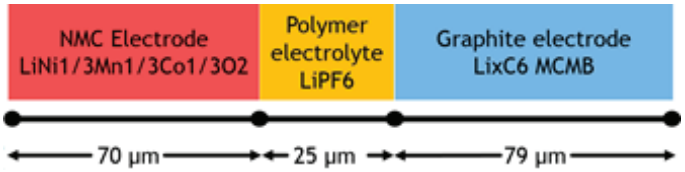

Figure 9. *1-D electrochemical battery cell model developed in COMSOL Multiphysics.*

20A, 40A, 60A, and 80A currents, generated by the 1-D battery cell model, are presented in Figure 10. Compared to the experimental data, the simulated voltage curves show a more significant initial voltage drop at the beginning of each discharge cycle. Specifically, the simulated voltages immediately after the discharging process begins (dropping from 4.2V) are 3.95V, 3.88V, 3.75V, and 3.73V for 20A, 40A, 60A, and 80A discharge currents, respectively. In contrast, the experimental starting voltages are 4.01 V, 3.90V, 3.91V, and 3.79V for the same currents. As illustrated in Figure 11, the differences between the simulated and experimental voltages after the discharge begins are generally under 0.1V for 20A and 40A currents, and under 0.2V for 60A and 80A currents during the first 85% of discharge. These discrepancies are considered acceptable. Additionally, the total discharge times (the duration required for the voltage to drop to 2.5V) for all discharge currents in the simulations are in close agreement with the experimental results, with a discrepancy of no more than 30 seconds.

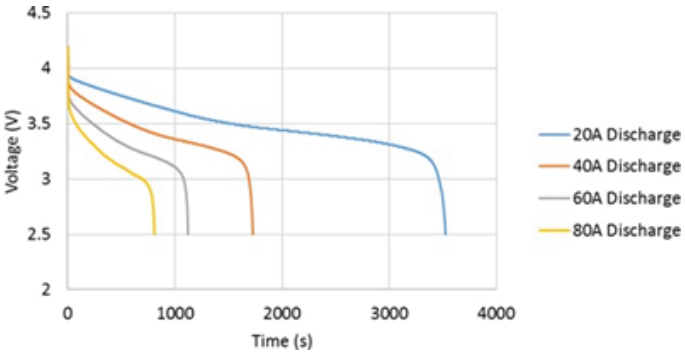

Figure 10. *COMSOL 1-D model simulated discharge voltage curves.*

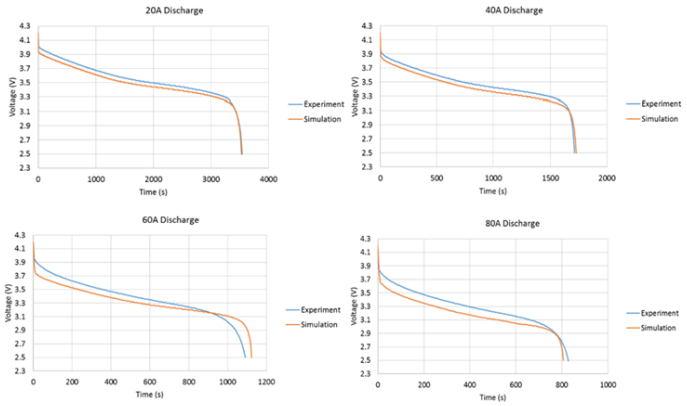

Figure 11. *Comparison of experimental and COMSOL 1-D Model simulated discharge voltage curves.*

The 1-D electrochemical battery cell model is then extended to a 3-D model in COMSOL. The steps to develop the 3-D electrochemical battery cell model are as follows:

1. Create the 3-D geometry: The COMSOL model includes the positive electrode, negative electrode, separator, two electrodes, and two current collectors, as shown in Figure 12. The dimensions of the electrodes and separator are based on the actual cell: the electrodes and separator have a length of 196 mm and a width of 127 mm, while the electrodes 1 and 2 measure 23 mm by 30 mm. The thickness of the positive and negative electrodes, as well as the electrode 1 and 2, is 3.5 mm, while the separator is 7 mm thick. These components form a "sandwich" structure.
2. Assign materials: The materials are specified as follows: LiPF6 for the polymer electrolyte, NMC for the positive electrode, graphite (LixC6 MCMB) for the negative electrode, and copper for the current collectors.
3. Set up the lithium-ion battery: The positive and negative porous electrodes are assigned to the corresponding cell geometry positions. "Current density" and "electric ground" are assigned to the current collectors. For the initial cell SOC, enter 1 (fully charged) or 0 (fully discharged). The battery cell capacity is set to 20 Ah. The testing current is applied to "electrode 1," with positive values for charging and negative values for discharging.
4. Add heat transfer module: The "heat transfer in solids" module is included, setting the ambient temperature as the initial battery temperature.
5. Select multi-physics parameters: The electrochemical heat source is selected for all domains, with lithium-ion battery physics for electrochemical effects and solids for heat transfer.
6. Generate physics-controlled mesh: A mesh is generated based on physics-controlled settings.
7. Define time-dependent simulation: Set the start time, stop time, and step length for the simulation. Use physics-controlled tolerance settings for the simulation accuracy.

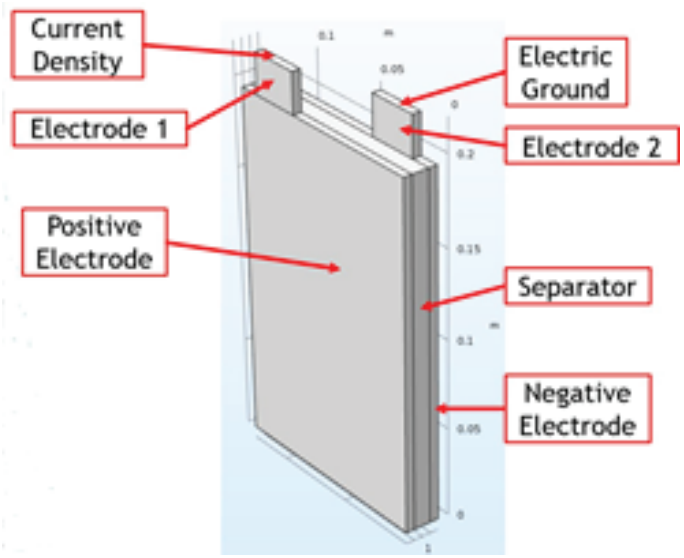

Figure 12. *3-D geometry of the battery cell developed in COMSOL Multiphysics.*

Figure 13 displays the simulated temperature distributions at the end of 20A, 40A, 60A, and 80A discharge cycles. The positive tab and its surrounding region consistently exhibit the highest temperatures, while the negative tab and its adjacent areas show slightly lower temperatures. As expected, the temperature gradually decreases with increasing distance from the cell tabs. The simulation results indicate a relatively uniform temperature distribution across the thickness of the cell. The temperature variation across the cell's thickness is minimal and can be considered negligible, given that the thickness is much smaller compared to the length and width of the cell.

As shown in Figure 13, the cell temperature rises with higher discharge currents at the end of the discharge process. During the 20A discharge, the temperature increases by approximately 3K, whereas it rises by as much as 22K during the 80A discharge. Additionally, the temperature variation across the cell becomes more pronounced as the discharge current increases. At the end of the 80A discharge, the temperature difference across the cell reaches around 8K.

A 40A charging simulation was conducted using the 3-D electrochemical battery cell model. As illustrated in Figure 14, the temperature distribution at the end of the charging test shows higher temperatures near the negative terminal (right tab in the figure), which contrasts with the temperature distribution observed at the end of the discharging test. This difference is

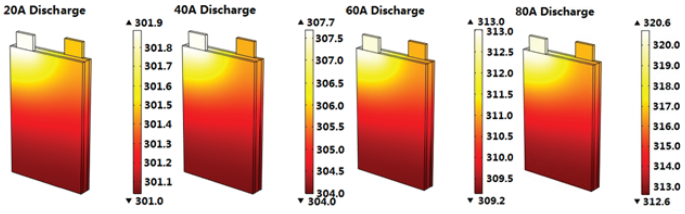

Figure 13. *COMSOL 3-D model simulated temperature distributions (K) at the end of 20A, 40A, 60A, and 80A discharge.*

due to the way lithium ions accumulate. During discharge, lithium ions accumulate on the positive electrode, while during charging, they accumulate on the negative electrode. This ion accumulation increases resistance, leading to higher temperatures in these areas. The right side of Figure 14 highlights that the current density is higher near the battery's terminals. The "sandwich" structure of the model (positive electrode, separator, and negative electrode) and the elevated current density near the tabs contribute to the observed temperature distribution.

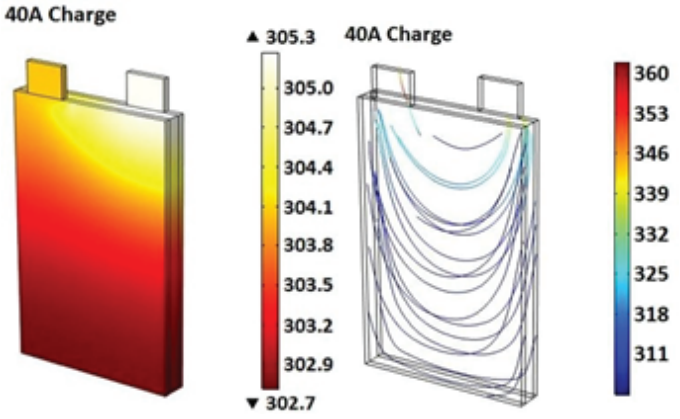

Figure 14. *COMSOL 3-D model simulated cell temperature distributions (K, left) and current density vectors (A/m², right) at end of 40A charge.*

Table 4 presents a comparison of temperature distributions between the simulation results (SIM) and experimental data (EXP), with "MID" and "END" referring to the midpoint and endpoint of the discharge process, respectively. The "DIF" columns show the differences between the simulated and experimental values, where positive values indicate that the simulated temperature is higher than the experimental temperature, and negative values indicate the opposite. The numbers in the "average" row represent the average absolute values of these differences. The average temperature differences between the simulations and experiments range from 0.4K to 1.3K. Given the close correlation between the simulated and experimental discharge voltage curves and temperature distributions, the cell model demonstrates acceptable accuracy and fidelity.

Table 4. *Comparison of experimental and COMSOL 3-D model simulated temperatures (K).*

Location	Time	20A DISCHARGE			40A DISCHARGE			60A DISCHARGE			80A DISCHARGE		
		SIM	EXP	DIF	SIM	EXP	DIF	SIM	EXP	DIF	SIM	EXP	DIF
Location#1	MID	300.5	299.8	0.7	304.0	303.3	0.7	307.2	306.7	0.5	312.6	310.3	2.3
	END	301.7	301.3	0.4	307.5	309.0	-1.5	312.9	311.9	1.0	319.9	317.3	2.6
Location#2	MID	300.4	299.6	0.8	304.0	303.5	0.5	307.1	306.4	0.7	312.4	310.9	1.5
	END	301.7	301.5	0.2	306.4	309.1	-2.7	311.6	312.5	-0.9	318.0	318.7	-0.7
Location#3	MID	300.4	299.8	0.6	303.9	303.2	0.7	307.1	307.1	0.0	312.2	309.7	2.5
	END	301.5	301.2	0.3	306.0	309.3	-3.3	311.3	311.3	0.0	316.5	316.9	-0.4
Location#4	MID	300.3	299.8	0.5	303.6	302.9	0.7	306.5	305.6	0.9	310.8	308.7	2.1
	END	301.4	301.5	-0.1	305.3	309.3	-4.0	310.5	312.2	-1.7	315.0	315.5	-0.5
Location#5	MID	300.3	299.8	0.5	303.5	302.7	0.8	306.4	305.8	0.6	310.7	309.4	1.3
	END	301.4	301.5	-0.1	305.2	308.0	-2.8	310.5	308.9	1.6	314.9	314.2	0.7
Location#6	MID	300.2	299.7	0.5	303.5	302.5	1.0	306.3	305.5	0.8	310.7	308.8	1.9
	END	301.4	300.8	0.6	305.2	305.2	0.0	310.4	310.4	0.0	314.9	314.5	0.4
Location#7	MID	300.0	299.7	0.3	302.8	302.6	0.2	305.8	305.7	0.1	309.3	309.0	0.3
	END	301.1	300.8	0.3	304.5	305.9	-1.4	309.5	308.8	0.7	313.3	313.2	0.1
Location#8	MID	300.0	299.5	0.5	302.8	302.7	0.1	305.8	305.5	0.3	309.3	309.0	0.3
	END	301.1	300.6	0.5	304.5	305.3	-0.8	309.5	308.5	1.0	313.3	313.2	0.1
Average				0.4			1.3			0.7			1.1

3-D Battery Model Developed in ANSYS Fluent

This section presents the simulation of heat generation and temperature distribution within the battery cell using a 3-D semi-empirical electrochemical model in the ANSYS Fluent. The model employed is the NTGK (Newman, Tiedemann, Gu, and Kim) empirical model, which is a semi-empirical electrochemical approach originally proposed by Kwon [15] and later validated by Kim et al. [16, 17]. The ANSYS Fluent NTGK battery model represents the battery as two parallel plate electrodes, as illustrated in Figure 15. This configuration mirrors the structure of a real battery, which consists of repeating units of positive and negative electrodes, polymer electrolytes, and separators. Figure 15 provides a schematic of the current flow during the charging process. It is assumed that the distance between the electrodes is small enough that the current flows perpendicular to the electrode surfaces. The modeling procedure and the equations used to calculate the potential and current density distributions on the electrodes are based on the works of Kwon et al. [15] and Kim et al. [16].

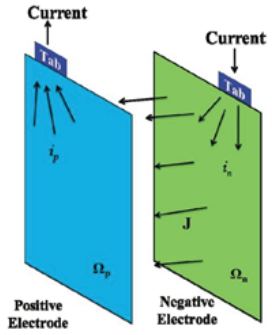

Figure 15. *Schematic diagram of the current flow in the ANSYS Fluent NTGK battery model during charge [16].*

The following equations are derived based on the continuity of the current on the electrodes [16].

$$\nabla \cdot \boldsymbol{i}_p - J = 0 \qquad (20)$$

$$\nabla \cdot \boldsymbol{i}_n + J = 0 \qquad (21)$$

Here, $\boldsymbol{i}_p$ and $\boldsymbol{i}_n$ represent the linear current density vectors (A/m) in the positive and negative electrodes, respectively, while J is the current density (A/m²) that flows through the separator from the negative electrode to the positive electrode. According to Ohm's law, $\boldsymbol{i}_p$ and $\boldsymbol{i}_n$ can be expressed as:

$$\boldsymbol{i}_p = -\frac{1}{r_p}\nabla V_p \qquad (22)$$

$$\boldsymbol{i}_n = -\frac{1}{r_n}\nabla V_n \qquad (23)$$

Here, r_p and r_n represent the resistances (Ω) of the positive and negative electrodes, respectively, while V_p and V_n denote the potentials (V) of the positive and negative electrodes, respectively. By substituting $\boldsymbol{i}_p$ and $\boldsymbol{i}_n$ into Equations (20) and (21), the following Poisson equations for V_p and V_n are derived.

$$\nabla^2 V_p = -r_p J \qquad (24)$$

$$\nabla^2 V_n = +r_n J \qquad (25)$$

The current density, J, is dependent on the potential difference between the positive and negative electrodes, $V_p - V_n$. The specific relationship is determined by the polarization

characteristics of the electrodes. In this study, the polarization expression proposed by [16] is used.

$$J = aY(V_p - V_n - U) \qquad (26)$$

Here, a represents the specific area of the electrode sandwich sheet, while Y and U are model parameters that can be determined from experimental data of voltage versus discharge current (Figure 16). In Figure 16, the dashed lines represent the data fitting curves. According to the works of [18], U corresponds to the intercept of these fitting lines, and Y is the inverse of the absolute value of the slopes. As depicted in Figures 17 and 18, both U and Y are expressed as functions of the DOD. Specifically, U is modeled by a cubic equation (Equation 27), while Y is represented by a quadratic function (Equation 28). The coefficients a_n in these equations are used to calculate U and Y, as detailed in Gu's work [18]. DOD, as shown in Equation 29, is calculated based on the total battery capacity, Q_T, in ampere- hours.

$$U = a_0 + a_1(DOD) + a_2(DOD)^2 + a_3(DOD)^3 \qquad (27)$$

$$Y = a_4 + a_5(DOD) + a_6(DOD)^2 \qquad (28)$$

$$DOD = \frac{\int_0^t Jdt}{Q_T} \qquad (29)$$

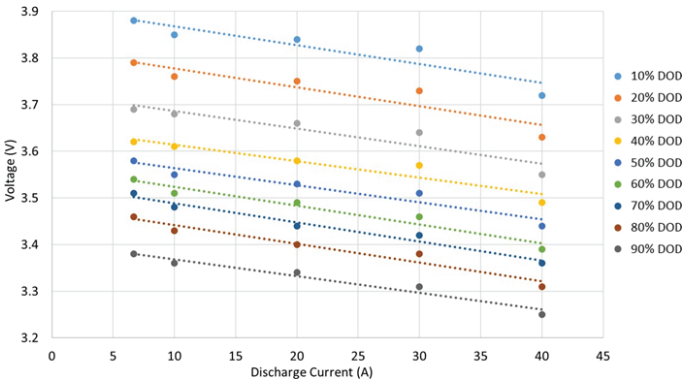

Figure 16. *Experimental voltage vs. discharge current data with fitting lines (dashed).*

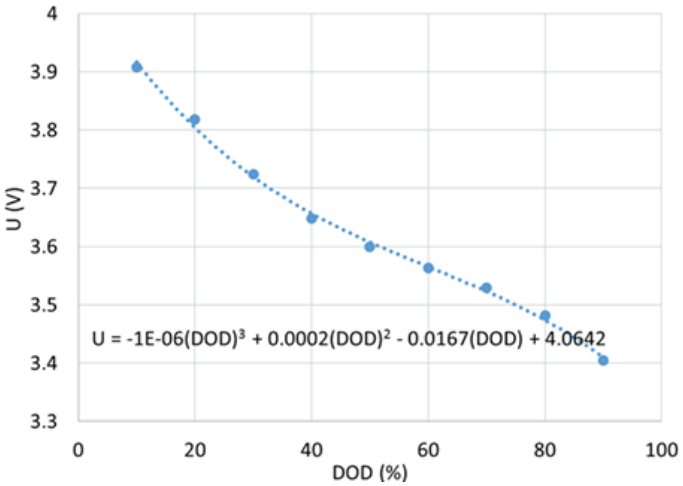

Figure 17. *Determination of U.*

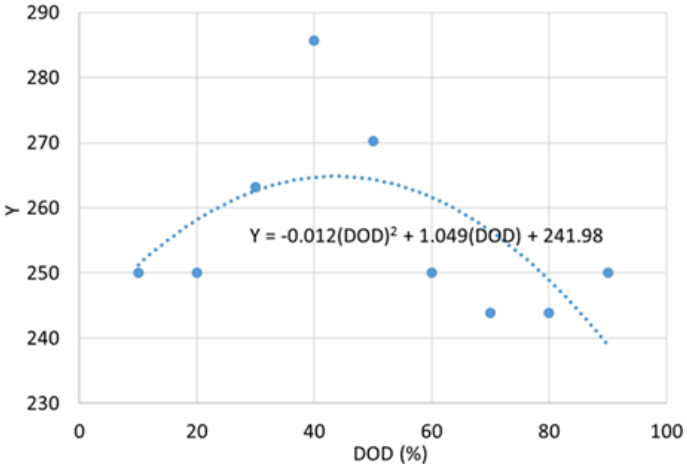

Figure 18. *Determination of Y.*

Equation 30 shows that energy sources consist of three types of heating, which are Joule heating, electrochemical reaction heating, and entropic heating:

$$\dot{q} = \sigma_+ \nabla^2 V_p + \sigma_- \nabla^2 V_n + J\left[U - (V_p - V_n) - T\frac{dU}{dT}\right] \qquad (30)$$

where $\sigma+$ and $\sigma-$ are the effective electric conductivities for the positive and negative electrodes, respectively. T is the temperature of the battery.

Next, the simulation model is set up through the following steps:

1. Model creation: A 3-D battery cell model is constructed in Design Modeler based on the actual dimensions of the ePLB-C020 cell used in the experiment (Figure 19). The cell dimensions are 196mm in length, 127mm in width, and 7mm in thickness. The positive and negative tabs are 30mm by 23mm, with a 2mm thickness.
2. Mesh generation: In this case, the battery cell geometry is meshed with 234,366 nodes and 204,672 elements in Mesh.
3. Fluent setup: The mesh file is imported into Fluent Setup. The "energy" and "MSMD battery model" are enabled. The "NTGK empirical model" is selected for its simplicity and semi-empirical nature. A nominal cell capacity of 20Ah is set, and the C-rate for each test is specified. The minimum and maximum stop voltages are set to 2.5V and 4.2V, respectively.
4. Model parameters: For the discharging simulation, an "initial DOD" of 0 is entered; for charging, an "initial DOD" of 1 is set. Coefficients for Y and U are entered as shown in the Figures 17 and 18. Active components, tab components, and electric contacts for the positive and negative tabs are assigned.
5. Material properties: Copper is assigned as the tab material. The active material properties inside the battery are set: density = 2092 kg/m³, specific heat = 678 J/kg-K, thermal conductivity = 18.4 W/m-K, and electrical conductivity = 3.541e+7 siemens/m. Diffusion coefficients are set for uds-0 and uds-1 as 1190,000 kg/m-s and 983,000 kg/m-s, respectively, based on the ANSYS requirement.
6. Boundary conditions: Thermal properties are set for all cell walls and tabs. Convection is chosen as the thermal condition, with a heat transfer coefficient of 8 W/m²-K and a free stream temperature of 298K (25°C), matching the test chamber conditions. Materials are assigned to the appropriate zones.

7. Solution settings: "SIMPLE" is used as the solution scheme, with hybrid initialization. The fixed time- stepping method is selected for the calculation, with a time step size of 60 seconds. The number of time steps is adjusted based on the C-rate for each test.

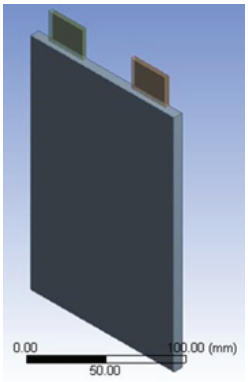

Figure 19. *3-D battery cell geometry constructed in ANSYS Fluent.*

Once the model is configured, continuous discharge tests at varying C-rates are simulated. The resulting simulated discharge voltage curves are shown in Figure 20. When compared to the experimental data, the discrepancies in the simulated voltage curves are within 10%.

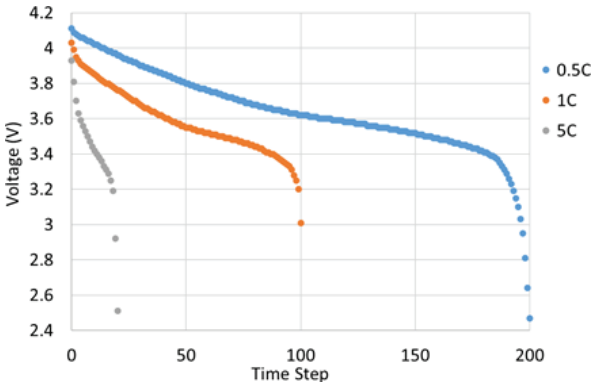

Figure 20. *Simulated discharge voltage curves for various C-rates using ANSYS Fluent 3-D battery cell model.*

Figure 21 shows the temperature contour plots generated using ANSYS Fluent. For each charging or discharging simulation, two contour plots are recorded: one at the midpoint and the other at the endpoint of the process. At the start of each simulation, the cell's surface temperature is uniformly set to 298.15 K. The plots reveal that regions near the positive and negative tabs consistently exhibit higher temperatures. Additionally, the temperature rise becomes more pronounced as the charging or discharging current increases. The variation in temperature across the cell surface also grows with increasing current.

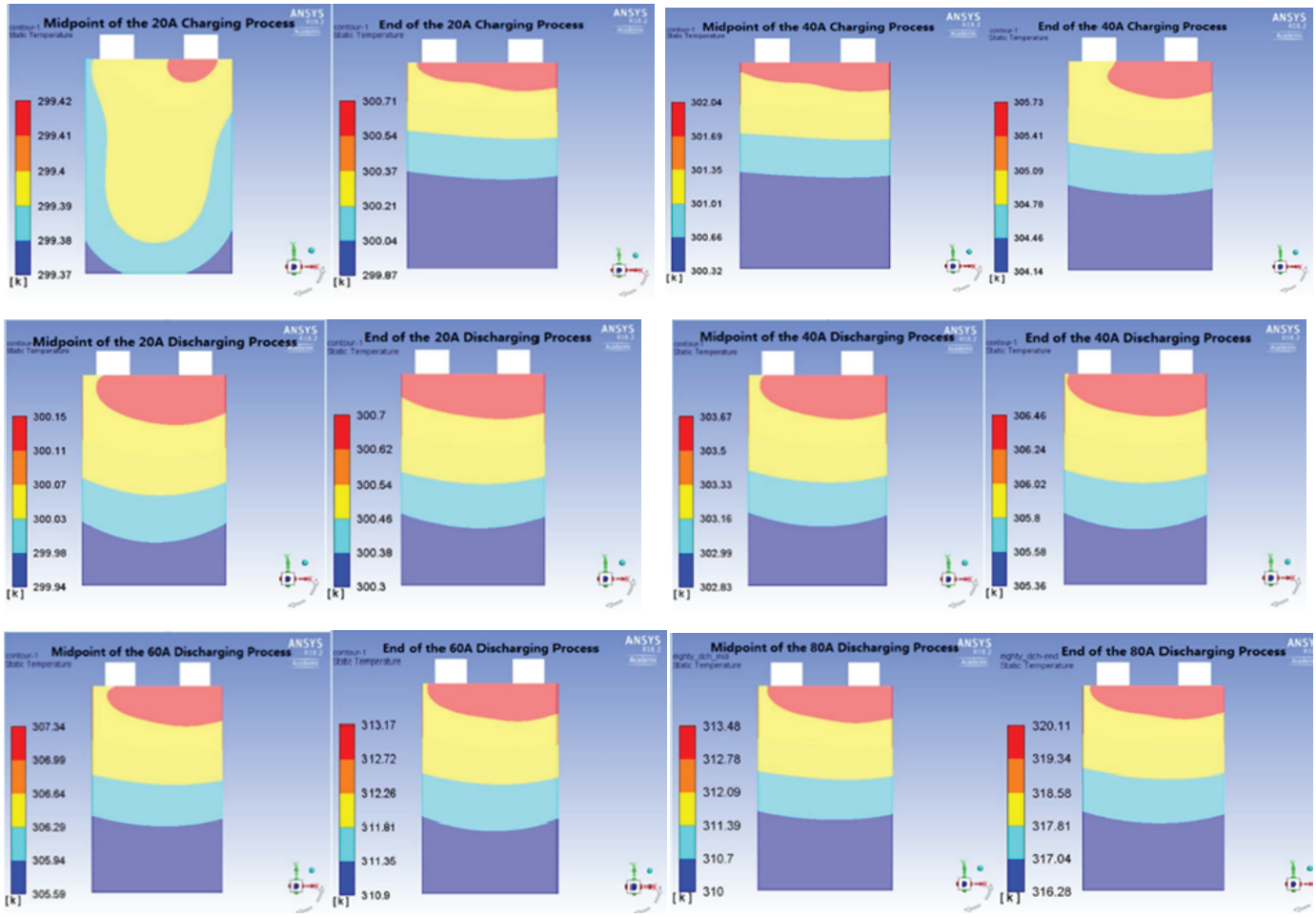

Figure 21. *Simulated temperature distribution on battery cell surface using ANSYS Fluent 3-D model.*

To validate the simulation results, experimental temperature data collected at eight locations during the midpoint and endpoint of each charging or discharging test, are utilized. The simulation results are compared with the experimental data and summarized in Table 5. The values in the "DIF" columns are obtained by subtracting the experimental temperatures from the simulated temperatures. A negative value indicates that the simulated temperature is lower than the experimental measurement, while a positive value indicates a higher simulated temperature.

As shown in the table, most temperature differences between simulation and experiment are less than 2 degrees. For the 60A and 80A discharge processes, the simulated temperatures are consistently higher than the experimental values. This discrepancy may be attributed to the battery cell's pouch case material. In the experiments, temperatures are measured on the external surface of the cell pouch case, whereas the simulated temperatures correspond to the active material inside the cell, which tends to be hotter than the cell's surface. Furthermore, the temperature differences increase with higher charging and discharging currents. During the 80A discharge process, the average temperature difference between simulation and experiment is approximately 2.5 degrees.

The total heat generation rate of the battery cell at the midpoint of each charging and discharging test is calculated using ANSYS Fluent and summarized in Table 6. The results indicate that higher terminal currents produce greater heat within the battery cell. Additionally, the heat generation rate during discharging is higher than that during charging at the same C-rate.

Next, a 3-D battery cell internal short-circuit model with varying penetration locations is developed in ANSYS Fluent using specifications and experimental data for validation. Simulated temperature distributions on the cell surface after an internal short-circuit event are compared to experimental results for model accuracy. The key steps for building the model are as follows:

1. Battery and electrochemistry setup: The "MSMD battery model" with the "NTGK empirical model" is enabled. A large external resistance (10,000 ohms) is applied to reflect no external current flow during penetration. Stop voltages are 2.5V and 4.2V, with initial DOD levels based on simulation conditions.
2. Material properties: Specific material properties (density, thermal conductivity, electrical conductivity, etc.) are defined for the active cell materials. User-defined scalar diffusion coefficients (uds-0 and uds-1) are set.
3. Boundary conditions: A convection thermal condition with an 8 W/m²-K heat transfer coefficient is applied to all walls, with a free-stream temperature of 25°C (ambient lab temperature).
4. Short-circuit configuration: Penetration locations are marked using the "Mark/Adapt" function. Short-circuit resistance at penetration points is applied using the "Patch" function and adjusted (initial value: 5e-7) to align simulated temperatures with experimental results. Penetration test with 50% battery cell SOC and Penetration Location 2 serves as the baseline, with experimental data from other penetration tests used for further validation.
5. Simulation run: A fixed time-stepping method with 30-second intervals is used. The number of steps corresponds to the desired simulation time (e.g., 10 steps for 5 minutes). Temperature data at specific time points are compared. This process ensures accurate simulation results aligned with experimental temperature distributions for various penetration cases.

Figure 22 presents the simulated temperature distributions on the battery cell surface for cells with 50% initial SOC and penetration at Penetration Location 1 (left), Location 2 (middle), and Location 3 (right), taken at 40, 30, and 40 minutes after penetration start, respectively. The results show that the highest temperatures occur at the penetration points, with temperatures decreasing gradually toward the surrounding areas. The temperature gradients are steeper near the penetration locations, while areas farther from these points exhibit minimal temperature variation.

***Table 6**. ANSYS Fluent calculated heat generation rate of the battery cell in the middle of each charge and discharge.*

	20A CHA	40A CHA	20A DCH	40A DCH	60A DCH	80A DCH
Total Heat Generation Rate (W)	1.611	5.012	3.694	7.692	11.533	16.706

***Table 5.** Comparison of experimental and ANSYS Fluent 3-D model simulated temperatures (K).*

Location	Time	20A CHARGE			40A CHARGE			20A DISCHARGE			40A DISCHARGE			60A DISCHARGE			80A DISCHARGE		
		SIM	EXP	DIF	SIM	EXP	DIF	SIM	EXP	DIF	SIM	EXP	DIF	SIM	EXP	DIF	SIM	EXP	DIF
Location#1	MID	299.4	300.3	-0.9	301.5	303.1	-1.6	300.1	299.8	0.3	303.5	303.3	0.2	307.1	306.7	0.4	312.7	310.3	2.4
	END	300.4	300.2	0.2	305.2	304.3	0.9	300.6	301.3	-0.7	306.3	309.0	-2.7	312.7	311.9	0.8	319.3	317.3	2.0
Location#2	MID	299.4	300.0	-0.6	301.6	303.0	-1.4	300.1	299.6	0.5	303.6	303.5	0.1	307.2	306.4	0.8	312.8	310.9	1.9
	END	300.5	300.0	0.5	305.4	304.3	1.1	300.7	301.5	-0.8	306.4	309.1	-2.7	312.9	312.5	0.4	319.4	318.7	0.7
Location#3	MID	299.4	300.3	-0.9	301.7	303.4	-1.7	300.1	299.8	0.3	303.6	303.2	0.4	307.3	307.1	0.2	312.8	309.7	3.1
	END	300.6	300.3	0.3	305.4	304.6	0.8	300.7	301.2	-0.5	306.4	309.3	-2.9	312.8	311.3	1.5	319.4	316.9	2.5
Location#4	MID	299.4	300.3	-0.9	300.7	302.7	-2.0	300.0	299.8	0.2	303.1	302.9	0.2	306.3	305.6	0.7	311.7	308.7	3.0
	END	300.1	300.3	-0.2	304.6	303.8	0.8	300.4	301.5	-1.1	305.8	309.3	-3.5	311.8	312.2	-0.4	317.7	315.5	2.2
Location#5	MID	299.4	300.3	-0.9	300.8	303.0	-2.2	300.0	299.8	0.2	303.2	302.7	0.5	306.4	305.8	0.6	311.8	309.4	2.4
	END	300.1	300.3	-0.2	304.7	303.8	0.9	300.4	301.5	-1.1	305.9	308.0	-2.1	312.0	308.9	3.1	317.8	314.2	3.6
Location#6	MID	299.4	300.0	-0.6	300.8	303.0	-2.2	300.0	299.7	0.3	303.1	302.5	0.6	306.4	305.5	0.9	311.7	308.8	2.9
	END	300.1	300.0	0.1	304.7	303.8	0.9	300.4	300.8	-0.4	305.8	305.2	0.6	311.8	310.4	1.4	317.7	314.5	3.2
Location#7	MID	299.4	299.9	-0.5	300.4	302.3	-1.9	300.0	299.7	0.3	302.9	302.6	0.3	305.7	305.7	0.0	310.5	309.0	1.5
	END	300.0	300.0	0.0	304.2	303.0	1.2	300.4	300.8	-0.4	305.5	305.9	-0.4	311.0	308.8	2.2	316.6	313.2	3.4
Location#8	MID	299.4	299.8	-0.4	300.4	302.3	-1.9	300.0	299.5	0.5	302.9	302.7	0.2	305.8	305.5	0.3	310.6	309.0	1.6
	END	300.0	299.8	0.2	304.2	303.3	0.9	300.4	300.6	-0.2	305.5	305.3	0.2	311.1	308.5	2.6	316.8	313.2	3.6
Average				0.3			0.5			0.2			0.7			1.0			2.5

Additionally, Penetration Locations 1 and 3 show higher peak temperatures and a wider temperature distribution range compared to Location 2. Figure 23 displays the simulated temperature distributions for Penetration Location 2 at 10% initial SOC (left) and 90% initial SOC (right), taken at 5 and 40 minutes after penetration, respectively. The results indicate that a higher initial SOC leads to higher surface temperatures.

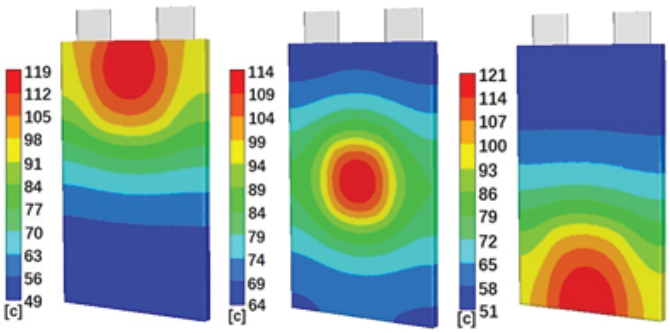

Figure 22. *ANSYS Fluent simulated temperature distributions on battery cell surface for Penetration Location 1 (left), 2 (middle), and 3 (right), at 40 minutes, 30 minutes, and 40 minutes after penetration start, respectively.*

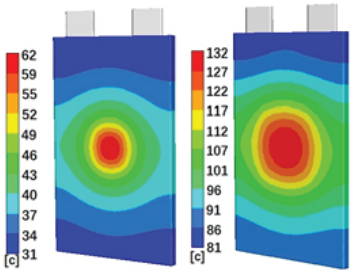

Figure 23. *ANSYS Fluent simulated temperature distributions on battery cell surface for Penetration Location 2 at 5 minutes (left) and 40 minutes (right) after penetration start, respectively.*

Furthermore, the area with the highest temperature is larger for the cell with 90% initial SOC compared to the cell with 10% initial SOC.

Table 7 compares simulated and experimental temperature data at Thermocouple Locations 1, 2, and 3 for selected time points across different cases. The "SIM" columns contain the simulated data, while the "EXP" columns show the experimental values. The "DIF" columns represent the differences between the two, where a positive value indicates the simulated temperature is higher than the experimental value, and a negative value indicates the opposite. Experimental data from Case 1 (50% Initial SOC, Penetration Location 2) are used for model calibration, while data from the remaining four cases are used for validation. In most cases, the differences between simulated and experimental temperatures are within six degrees Celsius, which is acceptable given the overall temperature variations. However, larger discrepancies are observed at Thermocouple Location 2 in Cases 2 and 3.

The total heat generation rate of the battery cell during various penetration tests at specific time points is calculated using ANSYS Fluent and summarized in Table 8. The results indicate that the penetration location has minimal impact on the total heat generation rate. Instead, the initial SOC of the battery cell plays a significant role in influencing the total heat generation rate during the penetration tests.

Table 8. *ANSYS Fluent calculated total heat generation rate of the battery cell in different penetration simulations at corresponding selected time point.*

Cell Initial SOC	Penetration Location	Selected Timing	Total Heat Generation Rate
50%	2	30 min	83.523 W
50%	1	40 min	86.416 W
50%	3	40 min	85.837 W
10%	2	5 min	24.291 W
90%	2	40 min	98.797 W

Table 7. *Comparison of experimental and ANSYS Fluent 3-D model simulated temperatures at Thermocouple (TC) Locations 1, 2, and 3 and at selected time points during penetration tests.*

	TC Location 1			**TC Location 2**			**TC Location 3**		
	SIM	**EXP**	**DIF**	**SIM**	**EXP**	**DIF**	**SIM**	**EXP**	**DIF**
50% Initial SOC Penetration Location 2	70.4	72.7	-2.3	103.8	100.2	3.6	73.1	71.7	1.4
50% Initial SOC Penetration Location 1	108.9	107.3	1.6	72.7	80.1	-7.4	52.8	52	0.8
50% Initial SOC Penetration Location 3	53.6	50.2	3.4	69.3	80.5	-11.2	108.8	110.3	-1.5
10% Initial SOC Penetration Location 2	33.3	35.5	-2.2	48.5	52.2	-3.7	35.1	33.4	1.7
90% Initial SOC Penetration Location 2	87.3	89.5	-2.2	122.4	117	5.4	91.5	89.2	2.3

Discussion and Summary

This paper explores the use of commercial software, including MATLAB/Simulink, COMSOL Multiphysics, and ANSYS Fluent, for modeling and simulating lithium-ion battery behavior. Each software platform offers unique advantages suited for different levels of simulation complexity and accuracy. MATLAB/Simulink excels in providing quick, 0-D lumped simulations of battery electrical and thermal responses. In contrast, COMSOL Multiphysics and ANSYS Fluent allow for more detailed, multidimensional simulations of electrical and thermal distributions within a battery cell, although they require more complex model setups and computational resources.

The MATLAB/Simulink model developed in this study is validated against experimental results obtained through a series of constant-current discharge tests at varying ambient temperatures and discharge rates. Comparisons between simulated and experimental discharge voltage curves show good agreement, particularly within the 0%–80% DOD range, where the deviations remain minimal. This range is especially relevant, as most battery applications operate within this DOD window to maintain longevity and performance. Beyond 80% DOD, larger discrepancies are observed due to the limitations in model parameters, particularly the simplified voltage representation. Nonetheless, the overall accuracy of the Simulink model is sufficient for many applications requiring fast simulation results.

The study also highlights the impact of temperature on battery performance. At elevated temperatures, experimental results reveal an increase in usable capacity and longer discharge durations compared to lower temperatures. However, the MATLAB/Simulink model does not fully account for this behavior, which underscores a limitation of simplified 0-D models. While sufficient for capturing general trends, these models are less effective at representing temperature-driven capacity variations that occur under extreme conditions.

More detailed multidimensional model simulations are performed using COMSOL Multiphysics and ANSYS Fluent. These tools provide insights into spatial variations of electrical and thermal properties across the battery cell. For example, the COMSOL simulations show that regions near the battery tabs experience higher temperatures and current densities during both charging and discharging processes. The temperature distribution across the cell is relatively uniform in the thickness direction due to the thin nature of pouch cells, but significant variations exist along the length and width of the cell. Higher discharge currents amplify these temperature gradients, with localized heating near the tabs becoming more pronounced.

Similarly, the ANSYS Fluent simulations capture detailed temperature distributions during charging and discharging processes. The results confirm that the temperature rise is more substantial at higher current rates and is concentrated near the positive and negative tabs. The simulations are validated against experimental temperature measurements taken at multiple locations on the battery cell surface. While the simulated temperatures generally align well with experimental results, slight discrepancies are observed, particularly at higher discharge currents. These differences are attributed to the fact that simulations calculate the internal material temperatures of the cell, while experimental measurements reflect the external surface temperatures. The pouch case material in the experimental setup may also influence heat dissipation, introducing additional variation.

This study further explores battery behavior under internal short-circuit conditions using ANSYS Fluent. Simulations of penetration-induced internal short-circuit events demonstrate that temperature hotspots occur at the point of penetration and gradually spread across the cell. The severity of the thermal response depends significantly on the battery's initial SOC, with higher SOC levels leading to greater temperature rises and larger affected areas. These findings underscore the importance of accurately modeling internal short-circuits to predict thermal runaway risks, which are critical for battery safety evaluations.

In summary, this work demonstrates the strengths and limitations of different commercial software tools for lithium-ion battery simulations. MATLAB/Simulink provides an efficient platform for quick, lumped-parameter simulations of battery electrical and thermal performance, making it ideal for scenarios requiring fast computational results and simplified models. On the other hand, COMSOL Multiphysics and ANSYS Fluent offer more detailed and accurate multidimensional simulations, which are capable of capturing complex spatial distributions of temperature and current density within the battery cell. These tools are essential for applications requiring a higher level of fidelity, such as safety assessments, thermal management system designs, and internal short-circuit analyses.

The results of this study validate the reliability of both 0-D and multidimensional models, depending on the requirements of the application. For general-purpose analysis and real-time simulations, MATLAB/Simulink remains a suitable choice. However, when more detailed insights into spatial variations and localized phenomena are needed, COMSOL and ANSYS provide a significant advantage. Moving forward, integrating multi-scale models that combine the efficiency of 0-D approaches with the accuracy of 3-D simulations could further enhance the ability to predict battery behavior under various operating conditions. Such advancements would help bridge the gap between simplified models and highly detailed simulations, ultimately improving the design, performance, and safety of lithium-ion batteries.

References

1. Kim, J. and Kowal, J. (2022) Development of a Matlab/Simulink Model for Monitoring Cell State-of-Health and State-of-Charge via Impedance of Lithium-Ion Battery Cells. Batteries, 8, 8. https://doi.org/10.3390/batteries8020008
2. Möller, M.C.and Krauter, S. (2022) Hybrid Energy System Model in Matlab/Simulink Based on Solar Energy, Lithium-Ion Battery and Hydrogen. Energies, 15, 2201. https://doi.org/10.3390/en15062201
3. Surya, S., Channegowda, J., Datar, S. D., Jha, A. S. and Victor, A. (2020) Accurate Battery Modeling Based on Pulse Charging using MATLAB / Simulink. 2020 IEEE International Conference on Power Electronics, Drives and Energy Systems (PEDES), Jaipur, India, pp. 1-3. doi: 10.1109/PEDES49360.2020.9379617
4. Şahin, M.E. and Blaabjerg, F. (2020) A Hybrid PV-Battery/Supercapacitor System and a Basic Active Power Control Proposal in MATLAB/Simulink. Electronics, 9, 129. https://doi.org/10.3390/electronics9010129
5. Zhu, Y., Li, K., Kang, E., Quan, T., Sun, T., Luo, J. and Zhao, S. (2023) Simulation Investigation on Thermal Characteristics of Thermal Battery Activation Process Based on COMSOL. Crystals, 13, 641. https://doi.org/10.3390/cryst13040641
6. Hu, Z., He, X., Restuccia, F. and Rein, G. (2023) Benchmarking Between COMSOL and GPYRO in Predicting Self-Heating Ignition of Lithium-Ion Batteries. Fire Technol, 59, 1319–1339.

https://doi.org/10.1007/s10694-022- 01335-x

7. Pozzato, G. and Onori, S. (2023) A General Matlab and COMSOL Co-simulation Framework for Model Parameter Optimization: Lithium-Ion Battery and Gasoline Particulate Filter Case Studies. SAE Technical Paper 2023-01-5047. https://doi.org/10.4271/2023-01-5047.
8. Goel, V. and Thornton, K. (2021) Enabling the Electrochemical Simulation of Li-ion Battery Electrodes with Anisotropic Tortuosity in COMSOL Multiphysics®. MethodsX, 8, 101425. https://doi.org/10.1016/j.mex.2021.101425
9. Parmar, M. P., Patel, D. R., Patel, V. K. and Patel, R. S. (2021) Thermal Simulation of Li-Ion Battery Pack Using ANSYS Fluent. Recent Advances in Mechanical Infrastructure: Proceedings of ICRAM 2020, 265-274. https://doi.org/10.1007/978-981-33-4176-0_22
10. Mačák, M., Vyroubal, P., Kazda, T., Capkova, D. and Maxa, J. (2022) Numerical Modelling of Discharging the Lithium-Sulphur Batteries in Ansys Fluent. Advances in Military Technology, 17(2), 163-177. https://doi.org/10.3849/aimt.01525
11. Wankhede, S. and Kamble, L. (2023) Performance Investigation of Electric Vehicle Battery Thermal Management System Using Nano Fluids as Coolants on ANSYS CFX Software. Energy Storage, 5(4), e420. https://doi.org/10.1002/est2.420
12. Mayıl, A. S. and Yetik, O. (2024) CFD Investigation of Pouchtype Lithium-ion Battery. Aircraft Engineering and Aerospace Technology, 96(7), 964-971. https://doi.org/10.1108/AEAT-03-2024-0076
13. "Simulink generic battery model," The MathWorks, 2024, https://www.mathworks.com/help/physmod/sps/powersys/ref/battery.html, accessed December 18, 2024.
14. COMSOL Inc., "COMSOL Batteries & Fuel Cells Module User's Guide (Version 5.3)," COMSOL Inc.: 2017.
15. Kwon, K. H., Shin, C. B., Kang, T. H. and Kim, C. S. (2006) A Two-dimensional Modeling of a Lithium- polymer Battery. Journal of Power Sources, 163(1), 151-157. https://doi.org/10.1016/j.jpowsour.2006.03.012
16. Kim, U. S., Yi, J., Shin, C. B., Han, T. and Park, S. (2011) Modeling the Dependence of the Discharge Behavior of a Lithium-ion Battery on the Environmental Temperature. Journal of The Electrochemical Society, 158(5), A611-A618. DOI: 10.1149/1.3565179
17. Kim, U. S., Shin, C. B. and Kim, C. S. (2008) Effect of Electrode Configuration on the Thermal Behavior of a Lithium-polymer Battery. Journal of Power Sources, 180(2), 909-916. https://doi.org/10.1016/j.jpowsour.2007.09.054
18. Gu, H. (1983) Mathematical Analysis of a Zn/NiOOH Cell. Journal of the Electrochemical Society, 130(7), 1459. DOI: 10.1149/1.2120009